Supplementary Information

Are we missing something when evaluating adsorbents for CO_2 capture at system level?

Hammed A. Balogun[a,b,c], Daniel Bahamon[a,b], Saeed AlMenhali[a,b], Lourdes F. Vega[a,b,†], Ahmed Alhajaj[a,b*]

[a] *Research and Innovation Center on CO_2 and H_2 (RICH), Khalifa University of Science and Technology, P.O. 127788, Abu Dhabi, United Arab Emirates.*

[b] *Chemical Engineering Department, Khalifa University of Science and Technology, P.O. 127788, Abu Dhabi, United Arab Emirates.*

[c] *School of Chemical and Biomolecular Engineering, Georgia Institute of Technology, Atlanta, GA 30332, USA.*

* Corresponding Author: ahmed.alhajaj@ku.ac.ae

† Corresponding Author: lourdes.vega@ku.ac.ae

S1. Adsorption equilibrium models

Grand Canonical Monte Carlo (GCMC) simulations were performed to generate adsorption isotherms of CO_2 and N_2. The pressures and temperatures were chosen to cover operating conditions relevant to post-combustion carbon capture processes. The dual-site Langmuir-Freundlich isotherm parameters for the 15%CO_2/85%N_2 binary mixture are provided in Tables S1a and S1b. The variables are the same as defined in the main paper (Eq. (8)) and in Eq. (S7) in this document.

Table S1a. Temperature-dependent fit parameters for CO_2 adsorption isotherms in 15%CO_2/85% N_2 binary mixture using a dual-site Langmuir-Freundlich model (273 K < T < 403 K, 0.01 kPa < P < 1200 kPa).

MATERIAL	$q_{Sat,A}$ (mol/kg)	b_{0A} (kPa^{-1})	E_A (J/mol)	v_A	$q_{Sat,B}$ (mol/kg)	b_{0B} (kPa^{-1})	E_B (J/mol)	v_B
Zeolite 13X (NaX)	1.9542	6.71×10^{-7}	36500	1	3.5240	3.11×10^{-8}	36000	1
Cu-BTC (HKUST-1)	13.4081	2.69×10^{-7}	24500	1.01	0	0	0	0
Mg-MOF-74	5.8601	8.20×10^{-8}	38500	1	9.0683	1.18×10^{-7}	24500	1
UTSA-16	3.7623	7.48×10^{-6}	22500	1.03	1.9567	1.13×10^{-7}	23500	0.9878
Activated Carbon	18.7791	1.56×10^{-6}	16000	1	18.1889	1.67×10^{-10}	15000	1

Table S1b. Temperature-dependent fit parameters for N_2 adsorption isotherms in 15%CO_2/85% N_2 binary mixture using a dual-site Langmuir-Freundlich model (273 K < T < 403 K, 0.01 kPa < P < 1200 kPa).

MATERIAL	$q_{Sat,A}$ (mol/kg)	b_{0A} (kPa^{-1})	E_A (J/mol)	v_A	$q_{Sat,B}$ (mol/kg)	b_{0B} (kPa^{-1})	E_B (J/mol)	v_B
Zeolite 13X (NaX)	0.1318	2.5129×10^{-4}	12000	1	0	0	0	1
Cu-BTC (HKUST-1)	2.3419	2.0376×10^{-6}	15500	1	0	0	0	1
Mg-MOF-74	2.0110	3.2891×10^{-6}	16900	1	0	0	0	1
UTSA-16	0.0429	5.0828×10^{-6}	12000	1	0.0534	9.6477×10^{-6}	18500	1
Activated Carbon	7.6029	7.1974 x10-6	7000	1	6.1644	1.2009 x10-6	9500	1

For the binary mixture of 15 mol% CO_2 and 85 mol% N_2, the amount of the gas phase components that can be adsorbed onto by the respective adsorbents are presented for selected temperatures in Figure S1. These are obtained using the Equation S7 with parameters provided in Tables S1a and S1b.

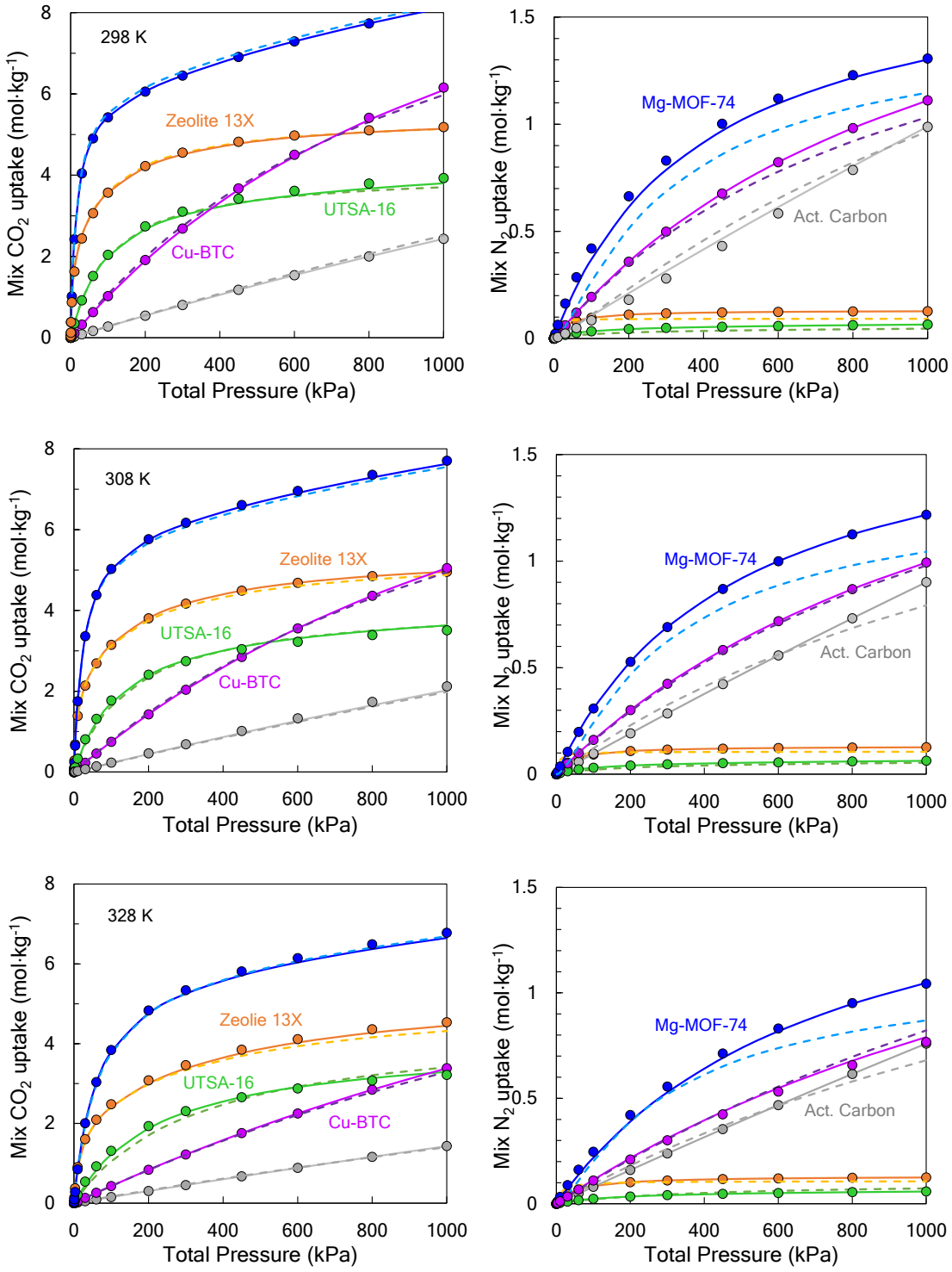

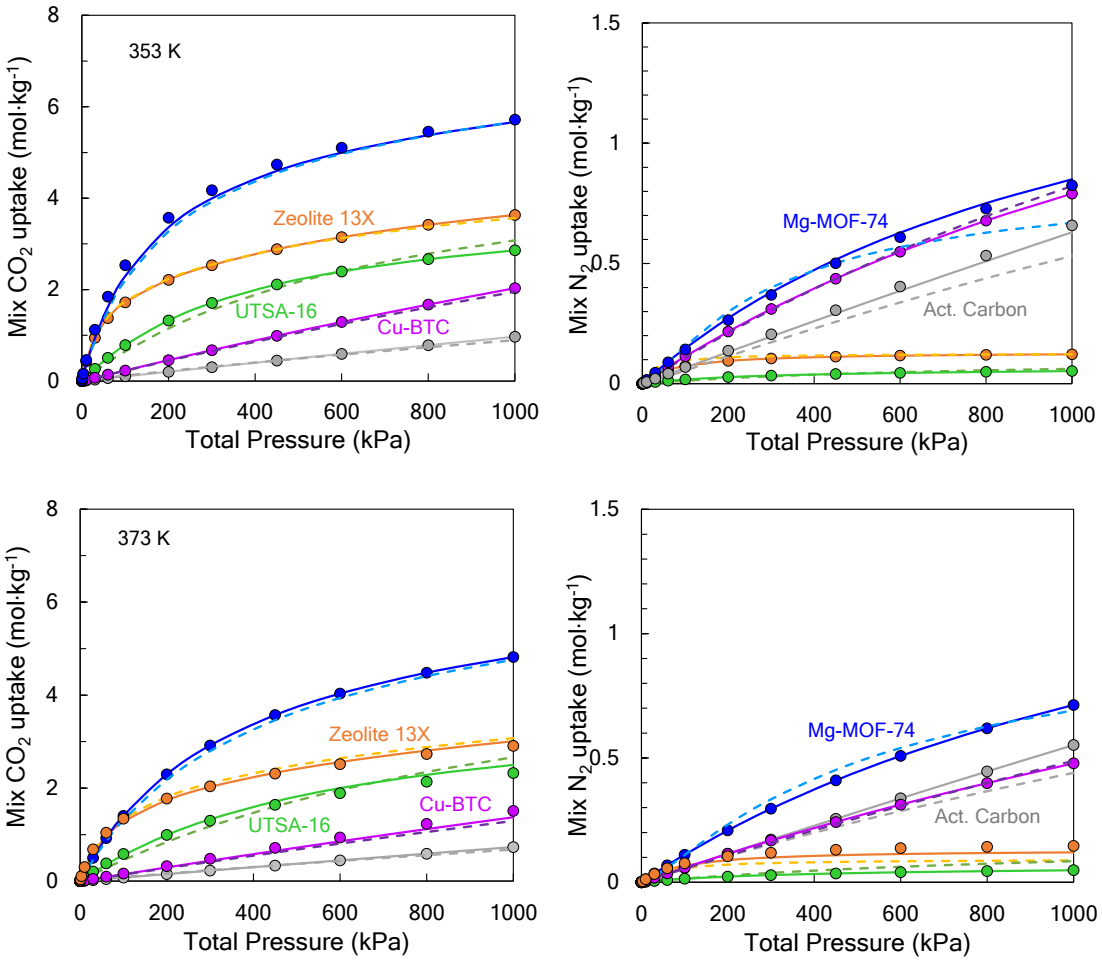

Fig. S1. Competitive loading capacities of CO_2 (left) and N_2 (right) as a function of temperature and total pressure for a binary mixture of 15 mol% CO_2 for different materials, using the fitted dual-site Langmuir-Freundlich model. [Symbols represent GCMC data (error bars are smaller than the symbols); competitive dual-site Langmuir (DSL) results are shown as dashed lines for comparative purposes].

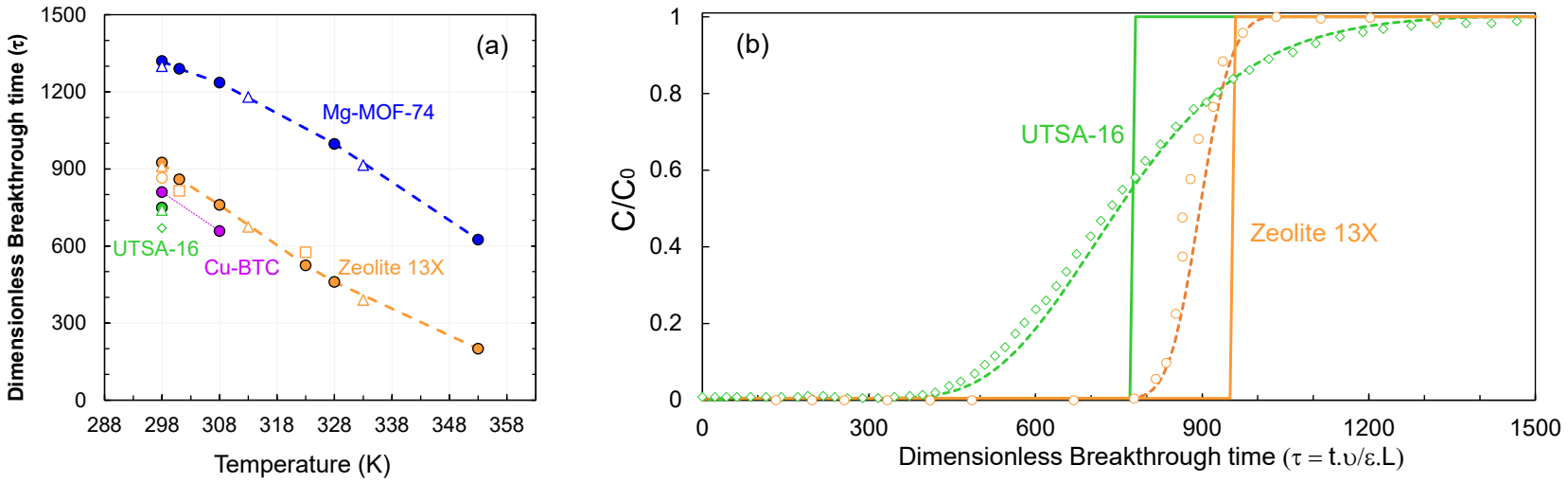

Fig. S2. **(a).** Comparison of dimensionless breakthrough times for studied adsorbent materials at atmospheric pressure and different temperatures: filled symbols represent obtained values from GCMC data, empty triangles are calculated values from Krishna and van Baten[1], empty diamonds correspond to experimental data from Masala et al.[2], and empty circles are experimental data from Dantas et al.[3] **(b)** Validation of dimensionless breakthrough curves for zeolite 13X and UTSA-16, compared with experimental data (same symbols as in figure (a)): full lines represent calculated curves assuming plug flow in the model, and dashed lines were obtained after including the dispersion term and re-scaling for the use of binder in the adsorption columns. [Additional validation of adsorption isotherms can be found in our previous works[4–6]].

S2. Dimensional form of VSA bed modelling system

The dimensional form of the pressure/vacuum swing adsorption process is presented in Tables S2 and S3.

Table S2. Model equations for the P/VSA process

Component material balance	
$\frac{\partial y_i}{\partial t} = D_Z \frac{T}{P}\frac{\partial}{\partial z}\left(\frac{\partial}{\partial z}\left(y_i \frac{P}{T}\right)\right) - \frac{y_i \partial P}{P\,\partial t} + \frac{y_i \partial T}{T\,\partial t} - \frac{T}{P}\frac{\partial}{\partial z}\left(y_i u \frac{P}{T}\right) - \frac{RT}{P}\left(\frac{1-\varepsilon_b}{\varepsilon_b}\right)\rho_p\left(\frac{\partial q_i}{\partial t}\right)$	(S1)
(Overall material balance	
$\frac{1}{P}\frac{\partial P}{\partial t} = \frac{1}{T}\frac{\partial T}{\partial t} - \frac{T}{P}\frac{\partial}{\partial z}\left(\frac{uP}{T}\right) - \frac{RT}{P}\left(\frac{1-\varepsilon_b}{\varepsilon_b}\right)\rho_p \sum_1^{Ncomp}\frac{\partial q_i}{\partial t}$	(S2)
Energy balance equation	
$\left(\frac{1-\varepsilon_b}{\varepsilon_b}\right)\left(\rho_p C_{p,p} + \rho_p C_{p,a}\sum_i q_i\right)\frac{\partial T}{\partial t} = \frac{K_Z \partial^2 T}{\varepsilon_b\,\partial z^2} - \frac{C_{p,g}\partial(u\cdot P)}{R\quad\partial z} - \frac{C_{p,g}\partial P}{R\;\partial t} - \left(\frac{1-\varepsilon_b}{\varepsilon_b}\right)\rho_p C_{p,a} T \sum_1^{Ncomp}\frac{\partial q_i}{\partial t} - \left(\frac{1-\varepsilon_b}{\varepsilon_b}\right)\rho_p \sum_1^{Ncomp}\left((\Delta H)_{a,i}\cdot\frac{\partial}{\partial}\right.$ $\frac{2h_i}{\varepsilon_b r_i}(T - T_w)$	(S3)
Column wall energy balance equation	
$\rho_w C_{p,w}\frac{\partial T_w}{\partial t} = K_w\frac{\partial^2 T_w}{\partial z^2} + \frac{2h_i r_i}{r_o^2 - r_i^2}(T - T_w) - \frac{2h_o r_o}{r_o^2 - r_i^2}(T_w - T_a)$	(S4)
Pressure drop profile	
$-\frac{\partial P}{\partial z} = \frac{150\mu u}{d_p^2}\left(\frac{1-\varepsilon_b}{\varepsilon_b}\right)^2$	(S5)
Linear driving force (LDF) approximation	
$\frac{\partial q_i}{\partial t} = k_i(q_i^* - q_i)$ $k_i = \frac{c_i}{q_i^*}\frac{60\varepsilon_b D_P}{d_p^2}$	(S6)
Adsorption isotherm equation	

$$q_i^* = \frac{q_{i,sat,A} b_{i,A} P_i^{v_{i,A}}}{1 + b_{i,A} P_i^{v_{i,A}}} + \frac{q_{i,sat,B} b_{i,B} P_i^{v_{i,B}}}{1 + b_{i,B} P_i^{v_{i,B}}} \quad \text{(S7)}$$

$$b_{i,A} = b_{0i,A} exp\left(\frac{E_{i,A}}{RT}\right); \quad b_{i,B} = b_{0i,B} exp\left(\frac{E_{i,B}}{RT}\right)$$

Diffusion/hydrodynamic equation

$$D_P = \frac{D_M}{\tau_p} \quad \text{(S8)}$$

$$D_z = 0.7 D_M + 0.5 u_f d_p$$

Table S3. Boundary conditions used for studied P/VSA process.

$z = 0$	$z = L$	
Pressurization		
$D_z \frac{\partial y_i}{\partial z} = -u(y_{f,i} - y_i)$	$\frac{\partial y_i}{\partial z} = 0$	(S9a)
$P(t) = P_{ads} - (P_{ads} - P_{evac}) e^{-\lambda_p t}$	$u = 0$	(S9b)
$K_Z \frac{\partial T}{\partial z} = -\varepsilon_b u \rho_g C_{pg} (T_f - T)$	$\frac{\partial T}{\partial z} = 0$	(S9c)
$T_w = T_a$	$T_w = T_a$	(S9d)
Adsorption		
$D_z \frac{\partial y_i}{\partial z} = -u(y_{f,i} - y_i)$	$\frac{\partial y_i}{\partial z} = 0$	(S10a)
$u = u_f$	$P = P_{ads}$	(S10b)
$K_Z \frac{\partial T}{\partial z} = -\varepsilon_b u \rho_g C_{pg} (T_f - T)$	$\frac{\partial T}{\partial z} = 0$	(S10c)
$T_w = T_a$	$T_w = T_a$	(S10d)
Blowdown		
$\frac{\partial y_i}{\partial z} = 0$	$\frac{\partial y_i}{\partial z} = 0$	(S11a)
$u = 0$	$P(t) = P_{bd} + (P_{ads} - P_{bd}) e^{-\lambda_{bd} t}$	(S11b)
$\frac{\partial T}{\partial z} = 0$	$\frac{\partial T}{\partial z} = 0$	(S11c)
$T_w = T_a$	$T_w = T_a$	(S11d)
Evacuation		
$\frac{\partial y_i}{\partial z} = 0$	$\frac{\partial y_i}{\partial z} = 0$	(S12a)
$P(t) = P_{evac} + (-P_{evac}) e^{-\lambda_{evac} t}$	$u = 0$	(S12b)

$z = 0$	$z = L$	
$\frac{\partial T}{\partial z} = 0$	$\frac{\partial T}{\partial z} = 0$	(S12c)
$T_w = T_a$	$T_w = T_a$	(S12d)

The dimensionless groups contained in the main manuscript are defined below.

$$Pe = \frac{u_0 L}{D_z} \tag{S13}$$

$$Pe_H = \frac{\varepsilon_b u_0 L}{\left(\frac{K_z}{\rho_g C_{pg}}\right)} \tag{S14}$$

$$\varphi = \rho_p \frac{R T_0 q_{s,0} 1 - \varepsilon_b}{P_0 \quad \varepsilon_b} \tag{S15}$$

$$\Omega_1 = \frac{\left(\frac{K_z}{\varepsilon_b u_0 L}\right)}{\frac{1-\varepsilon_b}{\varepsilon_b}\left(\rho_p C_{p,p} + \rho_p C_{p,a} q_{s,0} \sum_1^{Ncomp} x_i\right)} \tag{S16}$$

$$\Omega_2 = \frac{\left(\frac{C_{pg} P_0}{R \ T_0}\right)}{\frac{1-\varepsilon_b}{\varepsilon_b}\left(\rho_p C_{p,p} + \rho_p C_{p,a} q_{s,0} \sum_1^{Ncomp} x_i\right)} \tag{S17}$$

$$\Omega_3 = \frac{\rho_p C_{pa} q_{s,0}}{\left(\rho_p C_{p,p} + \rho_p C_{p,a} q_{s,0} \sum_1^{Ncomp} x_i\right)} \tag{S18}$$

$$\Omega_{4,i} = \frac{\rho_p \frac{q_{s,0}}{T_0}(\Delta H_i)}{\left(\rho_p C_{p,p} + \rho_p C_{p,a} q_{s,0} \sum_1^{Ncomp} x_i\right)} \tag{S19}$$

$$\Omega_5 = \frac{\left(\frac{2h_i\,L}{r_i\,u_0}\right)}{(1-\varepsilon_b)\left(\rho_p C_{p,p} + \rho_p C_{p,a} q_{s,0} \sum_{1}^{Ncomp} x_i\right)} \tag{S20}$$

$$\pi_1 = \frac{K_w}{\rho_w C_{pw} u_0 L} \tag{S21}$$

$$\pi_2 = \frac{2r_i h_i \quad L}{r_o^2 - r_i^2 \rho_w C_{pw} u_0} \tag{S22}$$

$$\pi_3 = \frac{2r_0 h_0 \quad L}{r_o^2 - r_i^2 \rho_w C_{pw} u_0} \tag{S23}$$

S3. Economic modelling

The purchased costs of the equipment are estimated using the cost correlations outlined in [7–9].

Table S4. Instrument cost and costing factor[8] for equipment types considered in this study.

	Instrumentation cost (US $) [a]	PC_f	IC_f	Material of construction [b]
Compressor	2,500	1.35	2.5	Cast steel
Heat exchanger (cooler)	9,750	1.0	2.5	CS/CS
Cooling water pump	2,500	1.35	2.5	Cast steel
Adsorption column	44,250	1.7	2.5	SS
Vacuum pump (with motors)	2,500	1.0	2.5	CS
Control valves	–	1.0	–	CS

[a] Instrumentation costs presented are estimated in 2004

[b] CS – carbon steel, and SS – stainless steel 304. PC_f and IC_f represent purchase cost and instrumentation cost factors, and are dependent on the material of construction.

The total capital cost of the capture plant and compression train can be estimated using the sequential approach as highlighted in Table S5.[10] The average Chemical Engineering Process Cost Index (CEPCI) was used to obtain their corresponding costs values dated to 2019 using Equation S24.

$$\frac{Cost_{2019}}{Cost_{base\ year}} = \frac{CEPCI_{2019}}{CEPCI_{base\ year}} \quad \text{(S24)}$$

Table S5. Elements in calculating total capital cost of capture plant[8,10,11]

Elements	Value
Purchased equipment cost (E)	$E_i, \forall i = 1,\ldots, n$
Instrument cost (I)	$I_i, \forall i = 1,\ldots, n$
Direct equipment cost (DEC)	$\sum_i^n PC_{f,i}E_i + \sum_i^n IC_{f,i}I_i$
Indirect equipment cost (IEC)	31% × *DEC*
Inside Battery Limit Investment (ISBL)	*DEC* + *IEC*
Off sites (OS)	31% × *ISBL*
Process unit investment (PUI)	*ISBL* + *OS*
Engineering (Eng)	12% × *PUI*
Paid-up royalties (PUR)	7% × *ISBL*
Facility capital cost (FCC)	*PUI* + *Eng.* + *PUR*
Interest during construction	Interest rate × *FCC*
Start-up cost	1 month of Total operating cost
Total capital cost (CAPEX)	*FCC* + Interest + Start-up cost
Working capital (WC)	1 month of Total operating cost

Table S6 presents the main elements of the operating and maintenance cost. The variable cost comprises utilities consumption (mainly electricity and cooling water) and adsorbent replacement cost. The fixed component of the operating and maintenance cost consists of the cost for labour, maintenance, insurance, and overheads.[10]

Table S6. Elements for capture plant operating and maintenance cost estimation[10]

Elements	Value
Electricity	\$ 0.08/kWh
Cooling water	\$ 0.02/m^3
Steam	\$ 1.4/GJ [1]
Utilities (U)	Electricity + Cooling water + steam
Adsorbent replacement cost (ARC)	Adsorber packing cost / Replacement rate
Variable cost (VC)	$U + ARC$
Labour cost (L) [a]	$\frac{\$\ 3{,}022{,}200}{year}$ [12]
Maintenance (M)	$4\% \times PUI$
Taxes and insurance (T&I)	$2\% \times PUI$
Overhead (OH)	$1\% \times PUI$
Financial working capital (FWC)	$9\% \times WC$
Fixed operating and maintenance (FOM)	$L + M + T\&I + OH + FWC$

[a] A labour unit of \$ 34.50/hour is used, and the total labour cost includes 10% for supervision.

The physical properties and unit cost of the five (5) studied adsorbents are presented in Table S7. These materials include zeolite 13X,[13,14] MOFs Cu-BTC,[15–18] Mg-MOF-74,[15,18–20] ,UTSA-16,[2,18,21,22] and activated carbon.[23–25] The unit cost of zeolite 13X was obtained from [3,6]; and that of MOFs was assumed to be \$10/kg. All materials were assumed to degrade at same rate. The tortuosity factor is estimated as a function of the particle void fraction as presented in Farmahini *et al*..[26]

Table S7. Properties of different adsorbents used in this study[2,14–27]

Properties	Zeolite 13X	MOF Cu-BTC	Mg-MOF-74	MOF UTSA-16	Activated carbon
Voidage	0.350	0.745	0.518	0.514	0.52
Density (kg/m^3)	1130	948.8	914.88	1659	990.0
Diameter (mm)	2.60	0.015	0.014	2.0	0.105
Pore diameter (nm)	1.0	3.3	1.0	1.18	1.39
Heat capacity (J/kg.K)	1070	760	896	1000	844
Replacement rate (year)	1.5	1.5	1.5	1.5	1.5
Unit cost (\$/kg)	0.50	10.00	10.00	10.00	0.3

[a] The replacement rates are taken as that of zeolite 13X [6]

The assumptions made in the cost estimation of the solid-based carbon capture plant are as follows:

- Nitrogen oxides, sulphur oxides and water have been removed from the flue gas prior to feed into the capture plant. Thus, the capture cost does not include the cost of dehydration and for the removal of these gases.
- The capture plant operates for 350 days in a year.
- The capture plant is discounted at a rate of 5% and has a lifetime of 15 years

S4. GSA-based optimization of P/VSA processes with different adsorbents

Fig. S3 illustrates the trade-off between purity and recovery as obtained from the GSA-base process optimization for the base case material (*i.e.*, zeolite 13X). The region enveloped by a red rectangle signifies process conditions that meet the 90/95 recovery-purity target. Similar results are obtained for other materials and the lowest cost process conditions set is selected within this region (90/95 target) or near the DOE target for detailed techno-economic assessment towards a low-cost industrial scale CO_2 capture and compression.

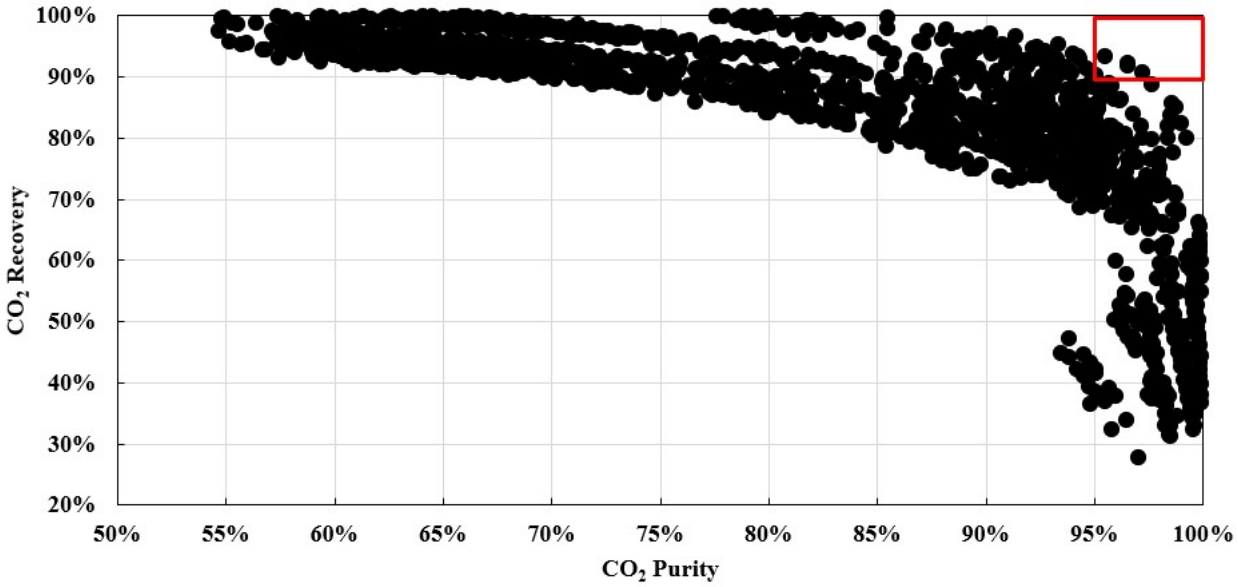

Fig. S3. Pareto plots of purity-recovery for zeolite 13X obtained from the GSA-based process optimization

The distribution of the investment and operating costs for the optimized performance of the different materials is presented in Table S8.

Table S8. Distribution of the ISBL and variable costs between components of the carbon capture plant and compression train for optimized performance of different adsorbents

	Zeolite 13Xv	Cu-BTC	Mg-MOF-74v	UTSA-16	Activated carbon	Zeolite 13Xp	Mg-MOF-74p
Total Investment Cost							
Feed blower and motors	15.10%	31.70%	7.62%	7.67%	36.37%	45.68%	41.15%
Feed heat exchangers	0.24%	0.54%	0.07%	0.51%	0.28%	0.15%	0.12%
Cooling water pumps	0.15%	0.26%	0.04%	0.18%	0.20%	0.20%	0.17%
Adsorption columns	17.69%	19.11%	17.25%	31.17%	3.54%	7.40%	5.04%
Blowdown vacuum pumps	10.06%	8.10%	38.96%	4.23%	25.30%	9.87%	17.08%
Evacuation vacuum pumps	18.00%	11.64%	18.48%	21.39%	18.88%	12.91%	20.15%
Control valves	6.69%	4.17%	1.36%	6.81%	0.49%	2.16%	0.48%
Post capture compressors	30.96%	23.60%	15.95%	26.78%	14.86%	21.19%	15.65%
Interstage coolers	1.11%	0.88%	0.28%	1.26%	0.09%	0.44%	0.16%
TOTAL (US M$)	**334.866**	**358.750**	**548.314**	**439.027**	**383.234**	**432.263**	**386.365**
Total Operating Cost							
Feed blower and motors	25.41%	41.16%	13.70%	10.08%	55.81%	58.58%	54.90%
Feed heat exchangers	0.21%	0.91%	0.14%	0.20%	1.26%	0.94%	0.91%
Cooling water pumps	0.15%	0.66%	0.10%	0.15%	0.92%	0.69%	0.66%
Adsorption columns	4.03%	20.36%	31.15%	42.89%	0.80%	1.25%	6.19%
Blowdown vacuum pumps	3.18%	0.44%	7.54%	0.49%	0.91%	1.67%	0.32%
Evacuation vacuum pumps	27.32%	14.68%	21.21%	20.92%	18.41%	15.07%	16.24%
Post capture compressors	39.03%	21.41%	25.71%	24.81%	21.48%	21.44%	20.42%
Interstage coolers	0.67%	0.38%	0.44%	0.46%	0.41%	0.37%	0.36%
TOTAL (US M$/yr)	**94.672**	**120.642**	**144.012**	**133.249**	**119.151**	**158.661**	**137.828**

S5. Correlation between molecular-based metrics and process performance

We carried out a correlation analysis of several material-centric metrics[27–32] presented in Equation S25 – S30 together with those already mentioned in the main manuscript. The results of the Pearson's correlation coefficient analysis are presented in Table S9. All working capacities and selectivities considered are those obtained from competitive adsorption and not of pure species.

$$Notaro's\ AFM = \Delta n_{CO_2} \cdot \frac{S_{CO_2}\big|_{ads}{}^2}{S_{CO_2}\big|_{evac}} \tag{S25}$$

$$Rege's\ AFM = \frac{\Delta n_{CO_2}}{\Delta n_{N_2}} \cdot \frac{S_{CO_2}\big|_{ads}{}^2}{S_{CO_2}\big|_{evac}} \tag{S26}$$

$$Adsorption\ Performance\ Indicator = \frac{\left(S_{CO_2}\big|_{ads} - 1\right) \cdot \Delta n_{CO_2}}{\left|\Delta H_{ads,CO_2}\right|} \tag{S27}$$

$$Selection\ Parameter = \frac{\Delta n_{CO_2}}{\Delta n_{N_2}} \cdot S_{CO_2}\big|_{ads} \tag{S28}$$

$$Separation\ Factor = \frac{\Delta n_{CO_2}}{\Delta n_{N_2}} \cdot \frac{y_{N_2}\big|_{feed}}{y_{CO_2}\big|_{feed}} \tag{S29}$$

$$Relative\ Selectivity = \frac{S_{CO_2}\big|_{ads}}{S_{CO_2}\big|_{evac}} \tag{S30}$$

$$Modified\ AFM = \Delta n_{CO_2}{}^a \cdot \Delta n_{N_2}{}^b \cdot S_{CO_2}{}^c\big|_{ads} \cdot S_{CO_2}{}^d\big|_{evac} \tag{S31}$$

This is a more general form of Eqs. S25, S25, S26, S28 and S30. If a = 1, b = -1, c = 2 and d = -1, then this proposed parameter is the same as Rege's AFM. If b=0, then it is Notaro's AFM, etc.. The correlation coefficients are obtained as the Pearson correlation coefficients between two

variables (e.g., working capacity and purity as defined by first numerical cell in Table S9). With the first variable (as array of a molecular-based metric of all materials at optimized process conditions) as *x* and second variable (as array of a KPI value of all materials at optimized process conditions) as *y*, the correlation coefficient, r_{xy} is estimated as:

$$r_{xy} = \frac{\sum(x-\bar{x})(y-\bar{y})}{\sqrt{\sum(x-\bar{x})^2(y-\bar{y})^2}}$$

where $\bar{x}$ and $\bar{y}$ are the sample averages of *x* and *y* respectively.

Table S9. The correlation coefficients of different molecular-based metrics to KPIs of process performance for optimized conditions of the different materials. Modified AFM is first introduced in this study and gives good correlations with all KPIs. SER, TAC and CT represents specific energy requirement, total annualized cost and compression train respectively.

	Purity	**Recovery**	**Productivity**	**SER without CT**	**SER with CT**	**TAC without CT**	**TAC with CT**
Working Capacity	0.20	-0.30	**0.76**	**0.78**	**0.72**	**0.50**	0.39
Adsorption Selectivity	-0.15	**0.57**	-0.40	-0.45	-0.44	-0.38	-0.28
Evacuation Selectivity	-0.40	**0.56**	-0.32	**-0.60**	**-0.59**	**-0.51**	-0.40
Notaro's AFM	0.19	**0.51**	-0.27	-0.06	-0.06	-0.07	-0.01
Rege's AFM	**-0.57**	0.40	-0.14	**-0.54**	**-0.56**	-0.16	-0.09
Adsorption Performance Indicator	0.29	**0.52**	-0.12	0.15	0.14	0.01	0.04
Selection Parameter	0.00	**0.58**	-0.28	-0.20	-0.20	-0.17	-0.10
Separation Factor	-0.27	**0.55**	-0.31	-0.44	-0.45	-0.28	-0.19
Relative Selectivity	**0.64**	0.42	-0.27	0.30	0.31	-0.07	-0.04
SER without CT	**0.62**	-0.06	**0.68**	**1.00**	**0.99**	**0.58**	0.48
Modified AFM *	**-0.52**	**0.55**	-0.45	**-0.74**	**-0.72**	**-0.77**	**-0.68**

* where a = -2.4549, b = 0.1072, c = 0.0998, and d = 1.5489 upon parameter fitting

S6. Effect of pressurization time on P/VSA performance

As proposed in the case study presented in this work, the effect of varying the pressurization time is hereby presented in Fig. S4.

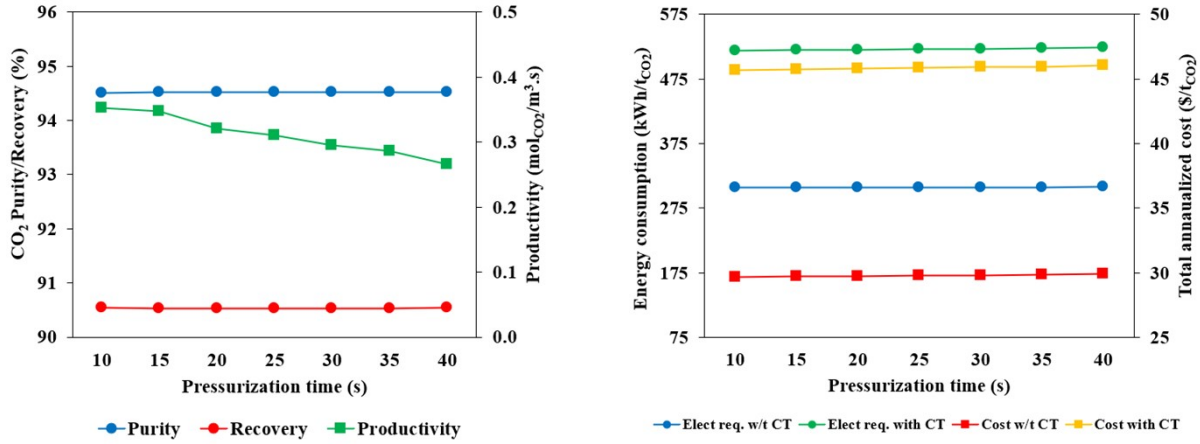

Fig. S4. Effect of duration of pressurization time step on process performance for optimized 13X PVSA operation. CT represents compression train after capture

References

1 R. Krishna and J. M. Van Baten, *Sep. Purif. Technol.*, 2012, **87**, 120–126.

2 A. Masala, J. G. Vitillo, F. Bonino, M. Manzoli, C. A. Grande and S. Bordiga, *Phys. Chem. Chem. Phys.*, 2016, **18**, 220–227.

3 T. L. P. Dantas, F. M. T. Luna, I. J. Silva, A. E. B. Torres, D. C. S. de Azevedo, A. E. Rodrigues and R. F. P. M. Moreira, *Chem. Eng. J.*, 2011, **172**, 698–704.

4 D. Bahamon and L. F. Vega, *Chem. Eng. J.*, 2016, **284**, 438–447.

5 D. Bahamon, A. Díaz-Márquez, P. Gamallo and L. F. Vega, *Chem. Eng. J.*, 2018, **342**, 458–473.

6 D. Bahamon, A. Ogungbenro, M. Khaleel, M. R. M. Abu Zahra and L. F. Vega, *Ind. Eng. Chem. Res.*, 2020, **59**, 7161–7173.

7 A. Alhajaj, N. Mac Dowell and N. Shah, *Int. J. Greenh. Gas Control*, 2016, **52**, 331–343.

8 J. R. Couper, W. R. Penney, J. R. Fair and S. M. Walas, *Chemical Process Equipment: Selection and Design*, Gulf Professional Publishing, 2nd edn., 2005.

9 M. Khurana, National University of Singapore, 2016.

10 A. Chauvel, *Manual of economic analysis of chemical processes : feasibility studies in refinery and petrochemical processes*, McGraw-Hill, Institut français du pétrole, 1981.

11 D. Danaci, M. Bui, N. Mac Dowell and C. Petit, *Mol. Syst. Des. Eng.*, 2020, **5**, 212–231.

12 N. Susarla, R. Haghpanah, I. A. Karimi, S. Farooq, A. Rajendran, L. S. C. Tan and J. S. T. Lim, *Chem. Eng. Res. Des.*, 2015, **102**, 354–367.

13 S. Krishnamurthy, V. R. Rao, S. Guntuka, P. Sharratt, R. Haghpanah, A. Rajendran, M. Amanullah, I. A. Karimi and S. Farooq, *AIChE J.*, 2014, **60**, 1830–1842.

14 S. Krishnamurthy, R. Haghpanah, A. Rajendran and S. Farooq, *Ind. Eng. Chem. Res.*, 2014, **53**, 14462–14473.

15 S. Shalini, S. Nandi, A. Justin, R. Maity and R. Vaidhyanathan, *Chem. Commun.*, 2018, **54**, 13472–13490.

16 K. S. Lin, A. K. Adhikari, C. N. Ku, C. L. Chiang and H. Kuo, in *International Journal of Hydrogen Energy*, Pergamon, 2012, vol. 37, pp. 13865–13871.

17 F. A. Kloutse, R. Zacharia, D. Cossement and R. Chahine, *Microporous Mesoporous Mater.*, 2015, **217**, 1–5.

18 S. Xiang, Y. He, Z. Zhang, H. Wu, W. Zhou, R. Krishna and B. Chen, *Nat. Commun.*, , DOI:10.1038/ncomms1956.

19 J. M. Huck, L. C. Lin, A. H. Berger, M. N. Shahrak, R. L. Martin, A. S. Bhown, M. Haranczyk, K. Reuter and B. Smit, *Energy Environ. Sci.*, 2014, **7**, 4132–4146.

20 D. A. Yang, H. Y. Cho, J. Kim, S. T. Yang and W. S. Ahn, *Energy Environ. Sci.*, 2012, **5**, 6465–6473.

21 H. Thakkar, S. Eastman, Q. Al-Naddaf, A. A. Rownaghi and F. Rezaei, *ACS Appl. Mater. Interfaces*, 2017, **9**, 35908–35916.

22 V. I. Agueda, J. A. Delgado, M. A. Uguina, P. Brea, A. I. Spjelkavik, R. Blom and C. Grande, *Chem. Eng. Sci.*, 2015, **124**, 159–169.

23 K. Uddin, M. Amirul Islam, S. Mitra, J. boong Lee, K. Thu, B. B. Saha and S. Koyama, *Appl. Therm. Eng.*, 2018, **129**, 117–126.

24 H. Khajuria, Imperial College London, 2011.

25 Y. C. Chiang, P. C. Chiang and C. P. Huang, *Carbon N. Y.*, 2001, **39**, 523–534.

26 A. H. Farmahini, D. Friedrich, S. Brandani and L. Sarkisov, *Energy Environ. Sci.*, 2020, **13**, 1018–1037.

27 K. T. Leperi, Y. G. Chung, F. You and R. Q. Snurr, *ACS Sustain. Chem. Eng.*, 2019, **7**, 11529–11539.

28 M. M. F. Hasan, E. L. First and C. A. Floudas, *Phys. Chem. Chem. Phys.*, 2013, **15**, 17601–17618.

29 US5810909A, 1998.

30 A. D. Wiersum, J. S. Chang, C. Serre and P. L. Llewellyn, *Langmuir*, 2013, **29**, 3301–3309.

31 S. U. Rege and R. T. Yang, *Sep. Sci. Technol.*, 2001, **36**, 3355–3365.

32 G. D. Pirngruber, L. Hamon, S. Bourrelly, P. L. Llewellyn, E. Lenoir, V. Guillerm, C. Serre and T. Devic, *ChemSusChem*, 2012, **5**, 762–776.